Design of a low-power all-optical NOR gate using photonic crystal quantum-dot semiconductor optical amplifiers

Hussein Taleb and Kambiz Abedi*

Department of Electrical Engineering, Faculty of Electrical and Computer Engineering, Shahid Beheshti University, Tehran 1983963113, Iran

**Corresponding author: k_abedi@sbu.ac.ir*

Received September 2, 2014; accepted September 29, 2014;
posted October 6, 2014 (Doc. ID 221945); published October 23, 2014

Design and simulation of a novel all-optical logic gate (AOLG) based on photonic crystal quantum-dot semiconductor optical amplifiers (PC-QDSOAs) is reported for the first time. For this purpose, a flat-band slow-light QD-based active photonic crystal waveguide (APCW) is designed and employed for implementation of an all-optical NOR gate in a symmetric Mach–Zehnder interferometer configuration. Then, the performance of the NOR gate is investigated using a comprehensive nonlinear state space model (NSSM). Simulation results demonstrate that PC-QDSOAs present an interesting platform for realizing ultracompact AOLGs with low power consumption. © 2014 Optical Society of America

OCIS codes: (130.5296) Photonic crystal waveguides; (230.5590) Quantum-well, -wire and -dot devices; (250.5980) Semiconductor optical amplifiers; (250.4745) Optical processing devices.
http://dx.doi.org/10.1364/OL.39.006237

All optical logic gates (AOLGs) are the building blocks of optical signal-processing devices, such as all-optical routers, all-optical switches, data encoders, and all-optical encryption systems [1]. Nonlinear effects either in optical fibers or in semiconductor optical amplifiers (SOAs) can be used for implementation of AOLGs. Although fiber-based AOLGs have the potential of operating at Tbits/s speeds, weak nonlinearity of fibers requires to launch high power as well as to use long interaction lengths [1]. On the other hand, SOAs have superior characteristics such as high nonlinearity, small size, and integration with other optoelectronic devices. These specifications make them popular candidates for use as nonlinear elements in AOLGs. In the literature, two general approaches are used to design SOA-based AOLGs. One is to use SOA in an optical interferometer configuration [2,3]. Another method is to use SOA with an optical bandpass filter [4]. Due to atom-like density of state (DOS) in quantum dots (QDs), SOAs with QD-active regions, also known as QDSOAs, have superior characteristics compared to their conventional counterparts [5]. However, the consumed power in QDSOA-based AOLGs is still a limiting factor for many AOSP devices. It has been proven that the slow light regime of photonic crystal waveguides can be used for decreasing the power consumption of QDSOAs, as well as enhancing the optical gain and phase changes [6,7]. It is demonstrated that QD-based photonic crystal Mach–Zehnder interferometer (MZI)-type switches can work at bit rates as high as 40 Gbits/s and switching energies as low as 10 fJ [8].

In this Letter, the design method and performance analysis of an all-optical NOR gate based on photonic crystal quantum-dot semiconductor optical amplifiers (PC-QDSOAs) is studied. It is well-known that the NOR gate is a universal gate since it can implement all kinds of logic functions. The designed NOR gate is a device with four inputs and consists of a symmetric MZI with two PC-QDSOAs placed in the upper and lower arms of the interferometer. In the following, we will discuss the design of different sections of the NOR gate. The time response of the designed NOR gate is then investigated using the nonlinear state space model of PC-QDSOA.

Design of PC-QDSOAs: PC-QDSOAs are based on a membrane slab geometry, wherein the population inversion in the active regions of amplifiers is achieved by passing current through laterally doped $p^+ - p - n^+$ structures [6]. The layer structure of the PC-QDSOA active regions is illustrated in Fig. 1. The active region is composed of five stacks of self-assembled InAs/GaAs QD layers that are separated from each other by 33-nm-thick p-doped GaAs spacer layers. Also, InAs QDs are covered with 5-nm-thick $In_{0.15}Ga_{0.85}As$ strain-reducing capping layer (SRCL). The thickness of the dielectric slab is 233 nm. Also, the lattice constant is $a = 330.8$ nm. More details about the designed PC-QDSOA are given in [6].

Design of photonic crystal optical power splitter (OPS): The OPS is a passive component and does not require any powering. Therefore, the PC slab in this region is made of the GaAs with a thickness of 233 nm. The OPS needs to be optimized for the wavelengths of data and probe signals. To design the PC structure of the OPS, we assume that the lattice constant of the PC lattice is similar with the lattice constant of the designed flat-band W1-PCW for the PC-QDSOAs, i.e., $a = 330.8$ nm [6]. To

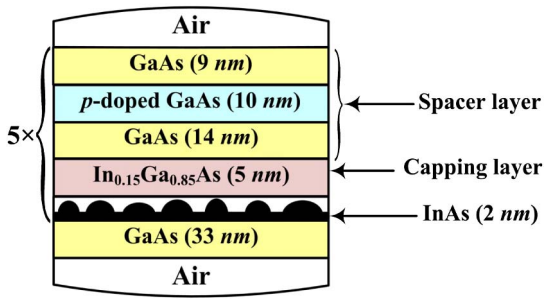

Fig. 1. Layer structure of the PC-QDSOA active region.

 © 2014 Optical Society of America

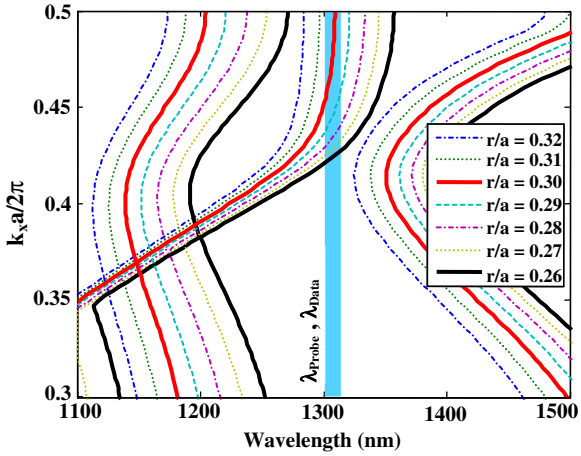

Fig. 2. Band structure of standard W1-PCWs, calculated using 2D-PWE for different radii of air holes ($n_{eff} = 2.905$).

evaluate the optical characteristics of PCWs, we use two-dimensional plane wave expansion method (2D-PWE) with effective index approximation to calculate the dispersion relations and optical mode profiles [9]. Figure 2 shows the calculated band structure for W1-PCWs with different radii of air holes.

As can be seen from Fig. 2, with decreasing the radius of air holes, the band edge of the guided mode in the W1-PCW moves to longer wavelengths. For a W1-PCW with $r = 0.26a$, both of the probe and data wavelengths are located in the linear regions of the dispersion diagram; a property which makes it suitable for designing the OPS. A wideband PC-based power splitter can be designed using an optimized Y-junction and two optimized 60-degree bends [10]. The geometry of the designed optical power-splitter is depicted in Fig. 3 (left). For an input field with a width of 0.5 μm and a wavelength of $\lambda_{Probe} = 1308$ nm, the amplitude of the magnetic field H_z is evaluated using 2D-FDTD method, as shown in Fig. 3 (right). As can be seen in this figure, the incident power is neatly divided between the output arms of the OPS.

Design of coupling region for PC-QDSOAs: In order to minimize the coupling loss between the output arms of the OPS and slow-light PCW of PC-QDSOAs, an efficient coupling region should be embedded between these two waveguides. As a result, the large group velocity modes of the output waveguides of the OPS can be transformed adiabatically into low group velocity modes of

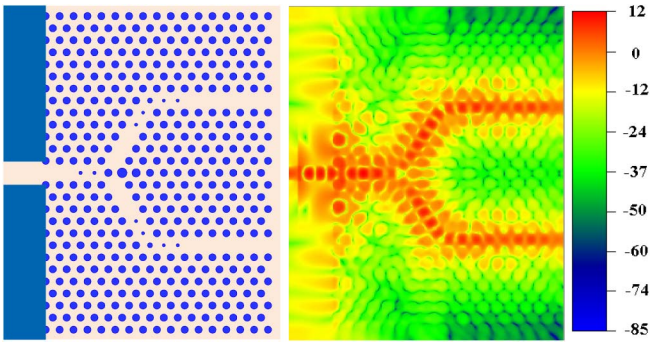

Fig. 3. Left, geometry of the optical power-splitter; Right, contour map of the magnitude of H_z (in logarithmic scale).

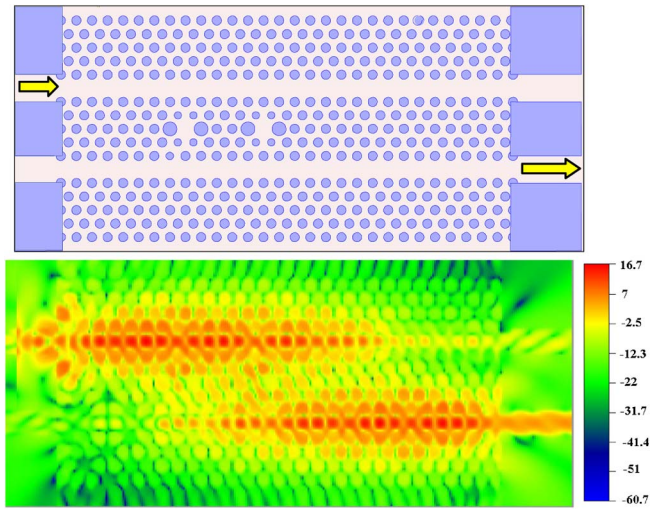

Fig. 4. Top, schematic of the channel add–drop filter; bottom, 2D-FDTD simulation results. The amplitude of the vertical magnetic field H_z is shown in the figure.

SL-APCWs. As can be seen from Fig. 2, the dispersion curve of the waveguide can be modified by changing the radii of air holes. Therefore, the group velocity mismatch between the OPS output waveguides and the SL-PCWs reduces using a number of periods, in which the radius of air-holes is increased from $r = 0.26a$ to $r = 0.3a$.

Design of channel add–drop filters for input multiplexer and output demultiplexer: As it is shown in [11], channel-drop filters (CDFs) can be implemented using two waveguides and an optical resonator system that support localized states. The geometry of the designed CDF is shown in Fig. 4.

In order to enhance the tunneling process between two W1-PCWs and the resonator system, the nonlinear region of the dispersion curve of W1-PCWs should be used in the structure of CDF. To do so, according to Fig. 2, the radius of air-holes in the PC lattice is chosen to be $r = 0.3a$. In our design, the point defects are created by removing one

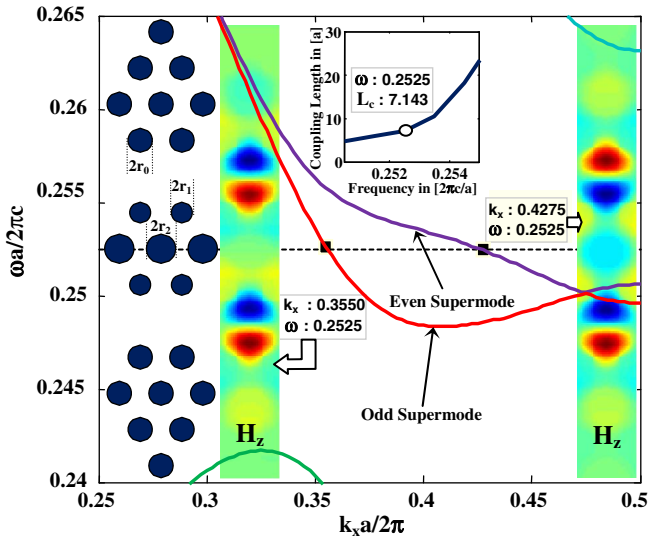

Fig. 5. Dispersion curves of the supermodes of the central section of the directional coupler.

hole in the triangular lattice. The resonance frequency of defect cavities is tuned by varying the radii of air holes beside the point defects. The radii of the larger and smaller air holes are 0.45a and 0.24a, respectively. Also, to satisfy the requirement for phase matching, i.e., $k_x d = n\pi + \pi/2$, the distance between two point defects is considered to be $d = 5a$. At the filtering wavelength, the resonance mode of the cavities couples effectively with modes of W1-PCWs.

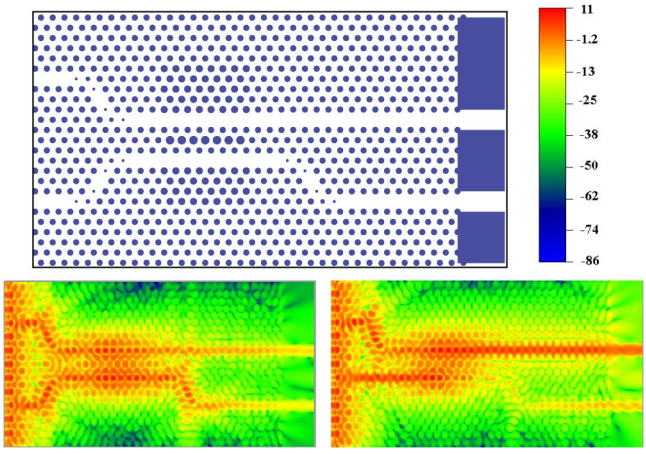

Fig. 6. Schematic diagram of the DC and FDTD simulation results for combination of in-phase and out-of-phase waves.

Design of output directional coupler: PCW-based directional couplers (DCs) are made of two PCWs that are brought close enough together to interact. This interaction splits the optical modes into odd and even symmetry supermodes and allows the transfer of optical power between the PCWs. The coupling length, i.e., the length at which the π phase change occurs, depends on the splitting of the odd and even supermodes [12]. The computational supercell of the designed DC and the magnetic field profiles (H_z) of the even and odd supermodes are illustrated in Fig. 5. The hole radii are $r_0 = 0.29a$, $r_1 = 0.25a$, $r_2 = 0.35a$. As shown in the inset of the figure, for the normalized frequency of $\omega a/2\pi c = 0.2525$, the coupling length is $L_c = 7a$.

The structure of the designed DC is shown in Fig. 6. Two signals from the upper and lower arms of the MZI recombine in the central section of the DC and then become separated at the output region of the DC. FDTD simulations are shown under the in-phase (left) and out of phase (right) conditions.

The final structure of the designed all-optical NOR gate is shown in Fig. 7. As can be seen from the figure, the input section of the NOR gate includes an OPS that divides the input power of the probe signal into two equal parts. Also, the clock signal is launched into the upper arm of the MZI. The two data signals A and B are multiplexed and injected into the lower arm of the MZI. In the

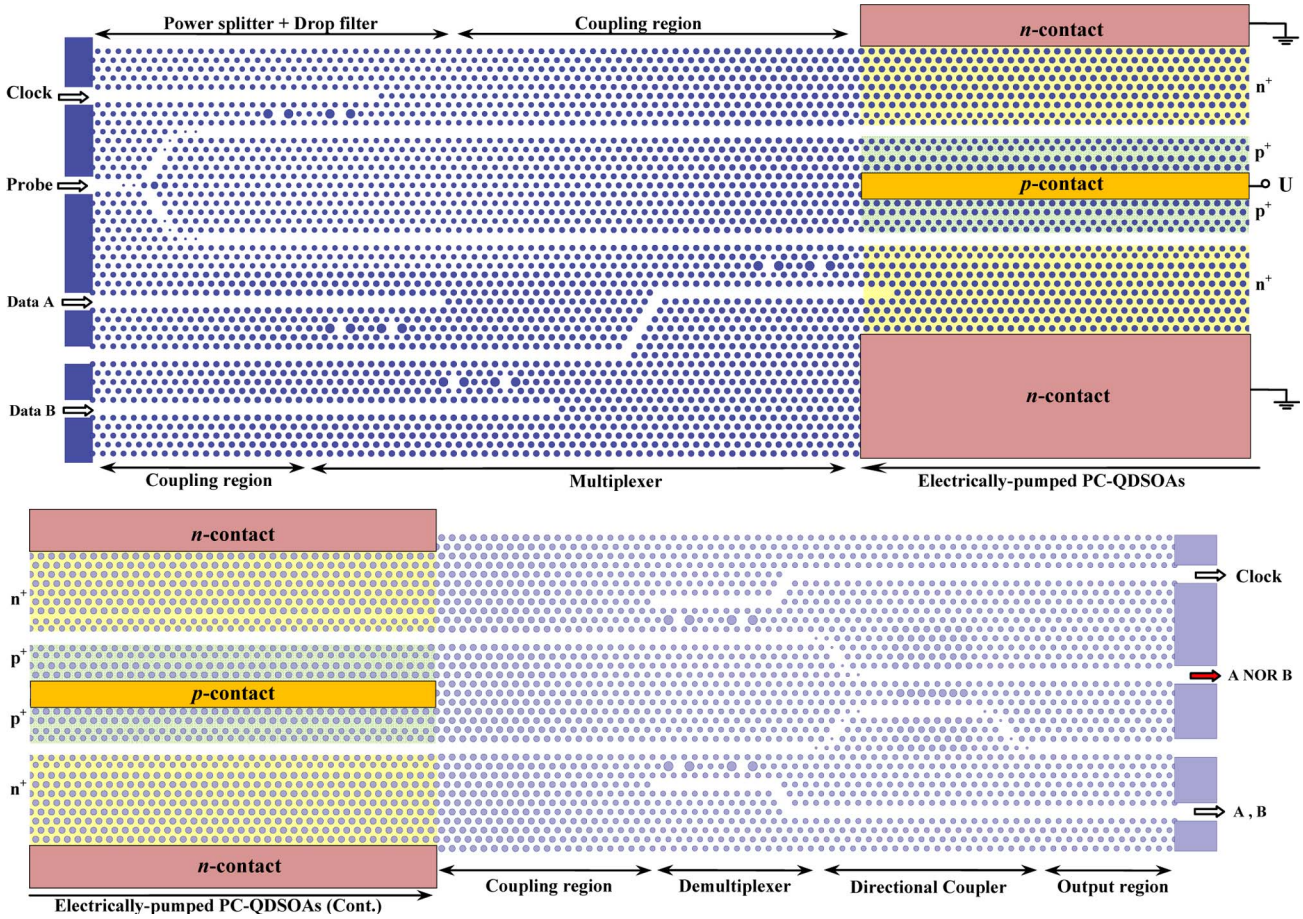

Fig. 7. Complete structure of the designed all-optical NOR gate using electrically-pumped PC-QDSOAs. The top figure represents the input section of the NOR gate and the bottom figure shows the output section of the device.

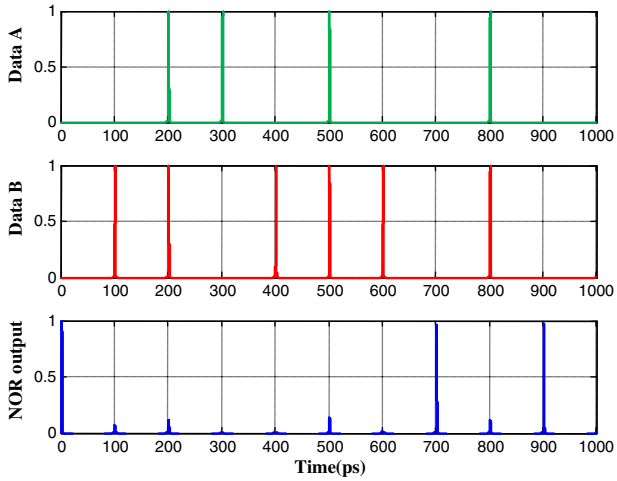

Fig. 8. NOR operation of an electrically-pumped PCQDSOA-MZI structure for 10 Gbits/s input bit sequence.

output section of the device, the clock and data signals are dropped from the MZI arms using two CDFs.

The designed AOLG works on the principle of the induced gain and phase changes on the probe wave in the presence of data and clock signals. If $A =$ "0" and $B =$ "0", because of existence of clock pulse in the upper arm, the MZI is unbalanced and consequently the output is "1". When $A =$ "1" and $B =$ "0", or $A =$ "0" and $B =$ "1", the MZI is balanced, and the output becomes "0". Finally, when $A =$ "1" and $B =$ "1", the MZI is semi-balanced and output is approximately equal to "0" [13]. To evaluate the performance of the NOR gate, the nonlinear state space equations of PC-QDOSA are solved numerically when two RZ pseudo-random bit sequence inputs at bit rates of 10 Gbits/s with an average power of 120 μW are applied to input A and input B. The time domain simulation of the device is shown in Fig. 8. The pump current of PC-QDSOAs is $I = 1.5$ mA, and $\lambda_{A,B} = 1310$ nm. A probe signal, which is a string of all "1" pulses with a repetition rate of 10 Gbits/s and an average power of $P_{Probe} =$ 20 μW, is split into two identical beams and propagates through two similar PC-QDSOAs located in the upper and lower arms of the MZI. The probe wavelength is $\lambda_{Probe} = 1308$ nm. Also, a clock signal that is a string of all "1" pulses with a wavelength of $\lambda_{Clock} = 1310$ nm and an average power of $P_{Clock} = 240$ μW is injected into the upper arm of the MZI. Figure 8 demonstrates the correct operation of the NOR gate.

The extinction ratio of the output signal is about 7 dB, which is limited by the slow phase recovery in PC-QDSOAs. To achieve a higher extinction ratio, optically-pumped PC-QDSOAs can be employed for implementation of AOLGs. It is shown that QDSOA-based AOLGs with optical pumping scheme can work at bit rates as high as 160 Gbits/s [14]. Therefore, the optical pumping scheme can be used to increase the operating speed of PC-QDSOA-based AOLGs by a factor of 10 and even more. Also, PC-QDSOA-based AOLGs can be cascaded to produce all-optical logic circuits. An all-optical logic circuit requires a number of additional devices to operate properly. The time delay blocks, optical filters, optical absorbers, and wavelength converters are among the most important building blocks of all-optical circuits [14].

In summary, we have proposed a novel all-optical NOR gate using PC-QDSOAs that can operate with a total power of less than 4 mW. To the best of our knowledge, this is the lowest power consumption among all-kinds of SOA-based all-optical logic gates that have been reported in the literature.

References

1. N. K. Dutta and Q. Wang, *Semiconductor Optical Amplifiers* (World Scientific, 2006).
2. E. Dimitriadou and K. E. Zoiros, Opt. Commun. **285**, 1710 (2012).
3. E. Dimitriadou and K. E. Zoiros, J. Opt. **14**, 105401 (2012).
4. M. Sahafi, A. Rostami, and A. Sahafi, Opt. Commun. **285**, 2289 (2012).
5. M. Sugawara, H. Ebe, N. Hatori, M. Ishida, Y. Arakawa, T. Akiyama, K. Otsubo, and Y. Nakata, Phys. Rev. B **69**, 235332 (2004).
6. H. Taleb and K. Abedi, IEEE J. Quantum Electron. **50**, 605 (2014).
7. H. Taleb and K. Abedi, IEEE Trans. Electron Devices **61**, 2419 (2014).
8. Y. Kitagawa, N. Ozaki, Y. Takata, N. Ikeda, Y. Watanabe, Y. Sugimoto, and K. Asakawa, J. Lightwave Technol. **27**, 1241 (2009).
9. M. Qiu, Appl. Phys. Lett. **81**, 1163 (2002).
10. M. Danaie and H. Kaatuzian, J. Opt. Soc. Korea **15**, 283 (2011).
11. S. Fan, P. R. Villeneuve, J. D. Joannopoulos, M. J. Khan, C. Manolatou, and H. A. Haus, Phys. Rev. B **59**, 15882 (1999).
12. D. M. Beggs, T. P. White, L. O'Faolain, and T. F. Krauss, "Design and fabrication of a photonic crystal directional coupler for use as an optical switch," in *ECIO '08*, Eindhoven, The Netherlands, 2008, pp. 379–382.
13. T. Nurmohammadi, K. Abbasian, M. J. Asadi, and D. Jafari, Optik Int. J. Light Electron Opt. **125**, 4023 (2014), doi: http://dx.doi.org/10.1016/j.ijleo.2014.01.119.
14. H. Taleb and K. Abedi, IEEE J. Sel. Top. Quantum Electron. **19**, 7600108 (2013).